Environmental Science Nano

The Influence of Surface Coating Functionality on the Aging of Nanoparticles in Wastewater

Journal:	*Environmental Science: Nano*
Manuscript ID	EN-ART-04-2019-000376.R1
Article Type:	Paper
Date Submitted by the Author:	15-Jun-2019
Complete List of Authors:	Surette, Mark; Oregon State University, School of Chemical, Biological, and Environmental Engineering Nason, Jeffrey; Oregon State University, Chemical, Biological and Environmental Engineering Kaegi, Ralf; eawag,

ENVIRONMENTAL SIGNIFICANCE STATEMENT

In an engineered nanomaterial's (ENM) life-cycle, wastewater treatment plants (WWTPs) represent important reactors where ENMs can be transformed. Although a large fraction of the ENMs entering WWTPs is accumulated in the sewage sludge / biosolids, a portion of the ENMs will be discharged to the environment. Ultimately, the physiochemical properties of these 'aged' ENMs are relevant when assessing their environmental fate. We investigated how the transformation processes of aggregation and corona formation are influenced by the surface coating applied to ENMs. We find that the initial properties of the surface coatings influence aggregation and corona formation. Furthermore, we find that these transformations persist as the aquatic chemistry of the surrounding media changes, e.g., when ENMs are transported through sequential treatment stages of a WWTP.

The Influence of Surface Coating Functionality on the Aging of Nanoparticles in Wastewater

Mark C. Surette[1,2], Jeffrey A. Nason[1,§], and Ralf Kaegi[2,]*

[1] School of Chemical, Biological and Environmental Engineering
Oregon State University, 116 Johnson Hall, Corvallis, Oregon 97331, United States

[2] Eawag, Swiss Federal Institute of Aquatic Science and Technology

Überlandstrasse 133, CH-8600 Dübendorf, Switzerland

ABSTRACT

Efforts to predict the environmental fate of engineered nanomaterials (ENMs) are frequently based on the physiochemical properties and behavior of the ENMs in their pristine, "as-produced" state. However, it is well-established that ENMs can be physically, biologically, and chemically transformed, resulting in altered physiochemical properties and behavior. Wastewater treatment plants (WWTPs) represent an important stage in an ENM's life-cycle where they can be transformed. To better understand the properties of ENMs discharged from WWTPs into surface waters, we investigated how the transformation processes of aggregation and corona formation are influenced by the surface coating applied to ENMs during their manufacture. Using 40 nm gold nanoparticles coated with polyethylene glycol, lipoic acid, or branched polyethylenimine as model ENMs, batch experiments were performed to investigate aggregation and corona formation during the primary clarification and activated sludge treatment stages. A tangential flow filtration system was used to evaluate if the initial transformations were altered as the aquatic chemistry of the background matrix was changed, mimicking the varying conditions ENMs would experience during transport through a WWTP. Using a combination of corroborative techniques including dynamic light scattering, phase analysis light scattering, ultraviolet-visible light spectroscopy, and transmission electron microscopy, we find that the model ENMs aggregated in each wastewater matrix, regardless of the initial surface coating. Differences in the UV-Vis spectra indicate that the nature of the corona acquired by the ENMs differed as a function of the surface coating of the pristine ENMs. In addition, initial ENM transformations during exposure to the influent wastewater persisted even as the background matrix changed. These results support the finding that ENMs discharged from WWTPs will not resemble their pristine analogs. Furthermore, the

corona acquired by ENMs in WWTPs may vary in relation to their pristine properties and be dictated by conditions during early stage exposures.

INTRODUCTION

To assess the implications posed by the increased use of engineered nanomaterials (ENMs), environmental fate models have been developed to identify the dominant exposure pathways and estimate exposure concentrations.[1–3] A fundamental concept underlying these models is that the physiochemical properties of ENMs can be used to predict their environmental behavior. Extensive research has been conducted to estimate the various input parameters used in these models.[4–6] Yet, much of this research inherently assumes that ENMs released to the environment will resemble their pristine, "as-produced" state. As discussed by Lowry et al. (2012), ENMs are likely to be transformed within natural environments, resulting in materials that have significantly different physiochemical properties than their pristine analogs. These transformation processes will also occur within engineered systems, such as sewers or wastewater treatment plants (WWTPs).

Transformations of colloids occur in natural and engineered environments through physical, chemical, and biological processes.[7–10] In the context of ENMs, significant attention has been given to investigating physical transformations via homo- and heteroaggregation[11–14] and chemical transformations via reduction-oxidation processes and dissolution[15–17]. In addition, the

adsorption of organic macromolecules including proteins, humic and fulvic substances to ENMs has been extensively investigated.[18–20]

Material Flow Analysis (MFA) modelling performed by various research groups have shown that WWTPs represent a common 'life stage' for many ENMs following their production and use.[21–29] While the majority of ENMs entering WWTPs are expected to heteroaggregate with suspended particulate matter (SPM),[30,31] the complete heteroaggregation and removal of all ENMs entering WWTPs is unlikely. Thus, WWTP effluent is one pathway through which ENMs are released to the environment. Indeed, numerous studies have detected ENMs in WWTP effluent.[32–36] To predict the environmental fate of ENMs and to assess the exposure to relevant forms of ENMs, the key factors and processes that drive ENM transformations have to be understood.

Various studies have investigated the transformations occurring to ENMs entering these engineered systems. Particular emphasis has been placed on the aggregation, sulfidation, and dissolution of AgNPs[30,32,33] and various metal oxide NPs, including, TiO_2[35,36], CeO_2[37], and SiO_2 NPs.[38,39] A common finding amongst these studies is that the ENMs that pass the WWTP and are discharged to surface waters possess properties that differ from their pristine state. As discussed by Salieri et al. (2018)[40], this observation has substantial implications for models that attempt to link ENM physiochemical properties to the processes affecting their environmental fate. Recent MFA modelling performed by Adam et al. (2018)[41] included data on the transformations of the ENM core material to estimate the form and annual release of two ENM types (AgNPs and TiO_2

NPs) to the environment. However, these authors noted the "almost complete lack of data" regarding transformations to the surface coatings applied to ENMs.

Continuing this line of inquiry, the surface coatings applied to ENMs during their manufacture, herein referred to as "engineered surface coatings", have been shown to influence the aggregation behavior of ENMs in both simulated and actual aquatic environments by mediating 'eco-corona' formation (i.e., the adsorption of natural organic macromolecules).[18,42–44] The focus of the current research was to investigate the role of engineered surface coatings in controlling aggregation and corona formation during conventional wastewater treatment (i.e., activated sludge process) and to understand the links, if any, between the properties of 'aged' ENMs and their pristine analogs in this context.

To accomplish this, three different 40 nm gold nanoparticles with covalently-bound engineered surface coatings were selected as model ENMs. Differently functionalized gold nanoparticles with well-defined particle sizes and functionalities provide an ideal platform to probe the impact of surface coating properties on ENM transformations while avoiding transformations to the core material, such as dissolution or sulfidation, that would confound such analysis. Corona formation and aggregation during individual WWTP stages were investigated using batch experiments containing filtered wastewater matrices from either the raw influent, nitrification, or denitrification stages of a pilot WWTP. Filtering these waters focused our assessment on the fraction of ENMs not removed via heteroaggregation with SPM. Corona formation and

(homo)aggregation were assessed using a suite of complementary and corroborative techniques, including ultraviolet-visible light spectroscopy (UV-Vis), dynamic light scattering (DLS), phase analysis light scattering (PALS), and transmission electron microscopy (TEM). These techniques probed changes related to the engineered surface coating including conformational changes or the adsorption of organic macromolecules, indicated whether the model ENMs aggregated, and revealed the resulting aggregate structure.

To simulate the effect of sequential wastewater treatment processes, a tangential flow filtration (TFF) system was used to exchange the wastewater matrix while keeping the model ENMs in the system. A combination of in-line UV-Vis and DLS detectors and off-line TEM analysis were used to assess corona formation and aggregation occurring over time as the composition of the wastewater medium changed. Results from these matrix exchange experiments were compared to the results of the batch experiments to assess whether subsequent exposures to different media affect the transformation processes.

MATERIALS AND METHODS

Engineered Nanomaterials

40 nm gold nanoparticles (AuNPs) with three different covalently-bound (thiol) engineered surface coatings were chosen as model ENMs: 5 kiloDalton (kDa) polyethylene gylcol (PEG), lipoic acid (COOH), and 25 kDa branched polyethylenimine (bPEI). All the AuNPs were purchased from

nanoComposix, Inc. (NanoXact 0.05 mg/mL). The measured and manufacturer reported characteristics of the pristine AuNPs are provided in Table 1. Further details regarding their characterization, including the conversion of the measured electrophoretic mobility (EPM) to the modelled zeta potential (ζ) values, are provided in the Supplementary Information.

Table 1. Measured and manufacturer reported properties of pristine AuNPs.

Surface Coating	Core Diameter, D_c (nm)	Intensity-Weighted Hydrodynamic Diameter, $D_{h,initial}$ (nm)	Electrophoretic Mobility, μ_E ([µm/S] / [V/cm])	Zeta Potential, ζ (mV)	Surface Plasmon Resonance, λ_{SPR} (nm)
PEG	40 ± 3	48.7 ± 0.6	-2.27 ± 0.4	-45.9 ± 8.1 (pH 5.5 ± 0.9)	523.3 ± 1.9
COOH	40 ± 5	50.0 ± 2.2	-2.06 ± 0.3	-41.7 ± 6.1 (pH 5.6 ± 0.5)	524.0 ± 0.0
bPEI	42 ± 5	51.7 ± 1.2	2.21 ± 0.4	44.6 ± 8.1 (pH 5.3 ± 0.3)	524.3 ± 0.7

Error bars indicate ± 95% confidence interval (D_c: N/A; $D_{h,initial}$: n = 34; μ_E/ζ: n = 9; λ_{SPR}: n = 3).

Preparation of Wastewater Matrices

Samples from the primary clarifier, denitrification, and nitrification stages were obtained from a pilot WWTP located at Eawag (Dübendorf, Switzerland). One liter of sample from a given reactor was collected prior to use each day between 9:00 – 10:00 a.m. It was found that the AuNPs readily heteroaggregated with SPM (Figure S1). To focus our assessment on the transformations caused by the aquatic chemistry of the wastewater matrix and represent the fraction of ENMs passing the WWTP, the SPM in the wastewater/mixed liquor samples was removed via centrifugation at

3,000 rpm (≈1,800*g* RCF) for 30 minutes (estimated particle size cutoff of ≈575 nm at $\rho_{particle}$ = 1.2 g/cm^3) followed by sequential filtration of the supernatant (≈900 mL) through 1 µm and 0.45 µm cellulose-acetate and 0.2 µm polycarbonate membrane filters (Sartorius). Details regarding the layout and operation of the pilot WWTP are discussed in Kaegi et al. (2011), with additional details regarding the properties of the wastewater matrices in Table S2.

Batch Experiments (Single Wastewater Matrix)

The colloidal stability of each AuNP type in the wastewater matrices was tracked using time-resolved dynamic light scattering (TR-DLS). Samples (V_{TOT} = 1 mL) containing a given filtered wastewater matrix (V_{WW} = 980 µL) were prepared in polystyrene micro-cuvettes (VWR) and dosed with 20 µL of a given AuNP type to a mass concentration (C_{NP}) of 1 mg Au/L. Upon dosing, the intensity-weighted hydrodynamic diameter (D_h) was recorded over an ≈45 minute period (160 measurements, each 15 seconds long) using a ZetaSizer Nano ZS (Malvern Panalytical). Using the TR-DLS data, the colloidal stability of the AuNPs was assessed by calculating the extent of aggregation ($D_{h,final}/D_{h,inital}$) according to the procedure described previously.[43]

Conformational changes to the engineered surface coating and/or the adsorption of organic macromolecules to the surface coating, as well as the aggregate structure, were investigated via time-resolved UV-Vis (TR-UV-Vis) using a Cary 60 UV-Vis Spectrophotometer (Agilent Technologies). Prior to sample analysis, the UV-Vis instrument was blank-corrected using 0.2 µm

filtered, 18.2 MΩ-cm Nanopure water (DDI; Barnstead). Then, the blank-corrected background spectrum of the wastewater matrix was measured by adding 9.8 mL (V_{TOT} = 10 mL) of the selected filtered wastewater matrix to a 50 mm light-path Quartz Suprasil® cuvette (Hellma Analytics) and measuring the absorbance (A) from λ = 400 – 800 nm at a rate of 10 nm/s. The wastewater matrix sample was then dosed with 0.2 mL of a given AuNP type to C_{NP} = 1 mg Au/L, gently mixed, and the absorbance of the sample was measured at 20-minute intervals over a period of 120 minutes. For each measurement, a background-corrected UV-Vis spectra and a background-corrected and normalized (A/A_{max}) UV-Vis spectra were generated (see Supplementary Information for details; Figure S2).

The surface charge of the AuNPs in the various wastewater matrices were investigated using phase analysis light scattering (PALS). Briefly, the electrophoretic mobility (EPM) of the model ENMs was measured using PALS and the resulting zeta potential (ζ) estimated as described in the Supporting Information. Samples (V_{TOT} = 1 mL) containing a given filtered wastewater matrix (V_{WW} = 980 µL) were prepared in polystyrene micro-cuvettes (VWR) and dosed with 20 µL of a given AuNP type to C_{NP} = 1 mg Au/L. After incubating for 30 minutes, ≈0.8 mL was transferred via sterile syringe to a Folded Capillary Zeta Cell (Malvern Panalytical) and the EPM of the sample was measured (5 measurements of 30 cycles each) using a ZetaSizer Nano ZS (Malvern Panalytical).

Finally, the size and structure of AuNP-containing aggregates was analyzed via transmission electron microscopy (TEM) using a scanning transmission electron microscope (STEM; HD2700Cs,

Hitachi). The microscope was operated at an acceleration voltage of 200 kV. The secondary electron (SE) and high angular annular dark field (HAADF) signals were used to assess the structure of the aggregates and the spatial arrangements of the primary particles within individual aggregates. Samples (V_{TOT} = 2 mL) containing a given filtered wastewater matrix (V_{WW} = 1.96 mL) were prepared in polystyrene micro-centrifuge tubes (VWR) and dosed with 0.04 mL of a given AuNP type to C_{NP} = 1 mg Au/L. The samples were then allowed to rest for 120 minutes. For the PEG- and COOH-AuNPs, 1 mL of the sample was then centrifuged onto a poly-L-lysine (0.1% w/v; Sigma-Aldrich) functionalized carbon grid (Cu 200 mesh, carbon coated, Plano GmbH) at 14,000 rpm (≈26,000*g* RCF) for 45 minutes. For the bPEI-AuNPs, 1 mL of the sample was centrifuged onto a glow discharged (ELMO, Cordouan Technologies) carbon grid (Cu 200 mesh, carbon coated, Plano GmbH) at the same conditions as the PEG- and COOH-AuNPs.

TFF Experiments (Changing Wastewater Matrices)

A wastewater matrix exchange process was developed to investigate the transformations occurring to a given AuNP type as the background wastewater matrix was changed, mimicking the varying aquatic chemistry ENMs would experience while transiting through a WWTP. To achieve this, a tangential-flow filtration (TFF) system equipped with a single-stage filtration unit was used (MMS Membrane Systems). The AuNPs were retained and continually cycled within the TFF system using a polyethersulfone (PES) membrane with a nominal pore size of 40 nm (GE Life Sciences), which was found to trap the AuNPs within the retentate while allowing sufficient flux of the background wastewater matrix through the membrane. Details regarding the operation

and testing of the TFF system are provided in the Supplementary Information (Figures S3 – S4 and Table S3).

Two sets of experiments were performed for each AuNP type using the TFF system—one wherein only the filtered influent wastewater matrix was used (baseline) and another wherein the background wastewater matrix was steadily changed to a mixture of influent, denitrification, and nitrification matrices (double matrix exchange). For each set of experiments, the same initial procedure was followed: (1) a 588 mL sample of filtered influent wastewater (V_{TOT} = 600 mL) was dosed with 12 mL of a given AuNP type to C_{NP} = 1 mg Au/L; (2) the sample was gently mixed and added to the TFF system reservoir; and (3) the TFF system was purged of air before continually operating with a transmembrane pressure (TMP) of 2-3 bar, a cross-flow velocity (V_s) of ≈1.4 cm/s, and at T = 19 – 20 ^{o}C. Samples of the retentate were continually removed from the TFF system at a rate of ≈2 mL/minute (F_R), while the flowrate of the permeate through the filter membrane varied between ≈0.4 – 0.6 mL/minute (F_P).

During the double matrix exchange, filtered wastewater from the denitrification reactor was added to the TFF system reservoir from t = 20 – 140 minutes at a rate of ≈2.5 mL/minute, matching the combined outflow from the system ($F_R + F_P$). From t = 40 – 240 minutes, filtered wastewater from the nitrification reactor was added to the TFF system reservoir. When both denitrification and nitrification wastewater were added to the TFF system (i.e., t = 40 – 140 minutes), the rate of addition of each matrix was reduced to ≈1.25 mL/minute so that the combined addition of the

denitrification and nitrification wastewater matrices matched the combined outflow from the TFF system ($F_R + F_P$). From t = 140 – 240 minutes, only the nitrification wastewater was added to the TFF system, at a rate of ≈2.5 mL/minute. This process, while not exactly mimicking the transport processes occurring in a full-scale WWTP, was deemed an appropriate compromise that both exposed the AuNPs to changing wastewater matrices over a reasonable amount of time and avoided excessive concentration or dilution of the AuNPs in the retentate.

The retentate removed from the TFF system, which contained the transformed ENMs, was pumped to a mixing cell that was continuously stirred via a magnetic stirrer. From there, samples were analyzed at 5-minute intervals via in-line DLS and UV-Vis detectors. The intensity-weighted hydrodynamic diameter (D_h) was measured via 3 measurements, each 20 seconds long using a ZetaSizer Nano ZS (Malvern Panalytical), while the UV-Vis spectrum was measured at λ = 400 – 800 nm at a rate of 1 nm/s using a Cary 60 UV-Vis equipped with a 40 mm light-path Torlon fiber-optic dip probe (Agilent Technologies). For each UV-Vis measurement, a background-corrected and normalized (A/A_{max}) UV-Vis spectra was generated (see Supplementary Information for details; Figure S5). The pH of the retentate was continuously monitored for the duration of the experiment. Upon completion of the experiment, ≈15 mL of the retentate was collected and analyzed via TEM according to the procedures described previously.

RESULTS AND DISCUSSION

Transformations in Single Wastewater Matrices

PEG-AuNPs. The extent of aggregation ($D_{h,final}/D_{h,inital}$) calculated from the TR-DLS measurements was used to determine if the ENMs aggregated in each wastewater matrix. Values of $D_{h,final}/D_{h,initial}$ ≈ 1 denote particle stability whereas $D_{h,final}/D_{h,initial}$ > 1 indicates that particles are aggregating, with 1.3D_h indicative of doublet formation.[45] The PEG-AuNPs aggregated in each wastewater matrix, as $D_{h,final}/D_{h,initial}$ was consistently > 1 (Figure 1). The TEM micrographs corroborate this finding and reveal that the PEG-AuNPs formed aggregates as large as a micrometer after incubating in each of the wastewater matrices for 120 minutes (Figures 2a-c).

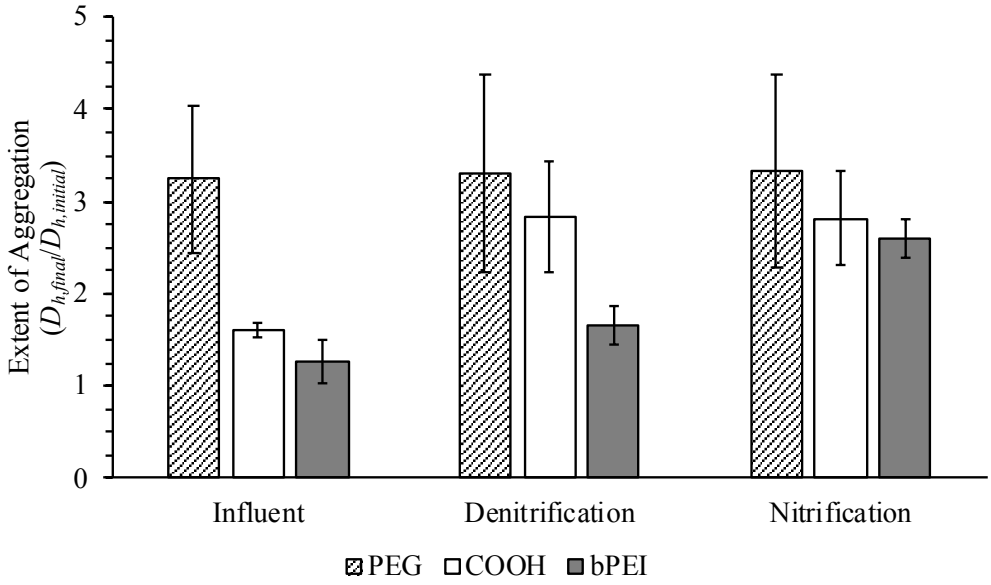

Figure 1. Extent of aggregation ($D_{h,final}/D_{h,initial}$) of each AuNP type in each matrix after ≈45 minutes. Error bars indicate ± 95% confidence interval (n = 3).

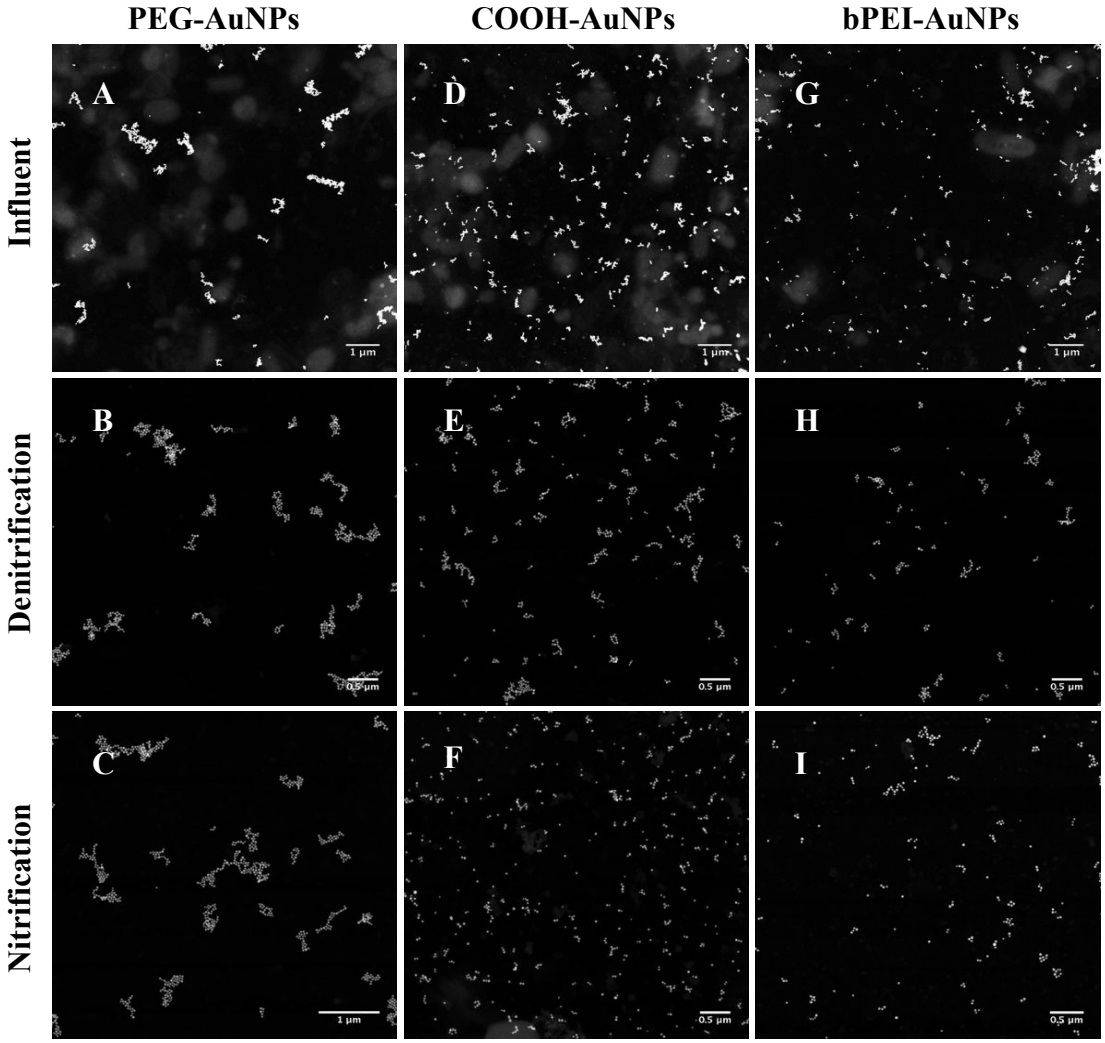

Figure 2. TEM-HAADF micrographs of (a-c) PEG-AuNPs, (d-f) COOH-AuNPs, and (g-i) bPEI-AuNPs in (top) influent (middle) denitrification and (bottom) nitrification wastewater matrices after incubating for ≈120 minutes.

The TR-UV-Vis spectra that were obtained after dispersing the PEG-AuNPs in each of the wastewater matrices possess several consistent features, illustrated in the example spectra shown in Figures 3a-c and the replicate spectra shown in Figures S11 – S13. First, there are two

distinct peaks in the UV-Vis measurements collected at $t \geq 20$ minutes: a primary peak located in proximity to λ_{SPR} (≈523 nm, Table 1, herein referred to as λ_{max}) and a secondary peak at longer wavelengths (λ'_{max}). The peak at λ_{max} was red-shifted relative to λ_{SPR} (Figure S10), although the amount was not statistically significant in the nitrification wastewater matrix. With the exception of one replicate measurement (Figure S12), the peak height at λ_{max} consistently decreased (see background-corrected spectra in Figures S11 – S13). Indications of the secondary peak are first evident within ≤ 20 seconds after the PEG-AuNPs were initially dispersed in each of the wastewater matrices, demonstrated by the "shoulder" occurring at $\lambda'_{max} \approx 620$ nm. At $t \geq 20$ minutes, this secondary peak was more pronounced, having higher absorbance than that measured at λ_{max}, and was located at $\lambda'_{max} \approx 750$ nm.

The quenching and red-shift observed at λ_{max} are characteristic patterns attributed to a change in the local dielectric permittivity (ϵ_r) near the AuNP surface. This change can occur through a number of mechanisms, including conformational changes to the molecular structure of the engineered surface coating and the adsorption of organic macromolecules to either the surface coating (overcoating) or directly to the AuNP surface (displacement).[46,47] These features are also produced when AuNPs aggregate such that very short center-to-center separation distances (d_s) occur and enable plasmon coupling between adjacent AuNPs.[48–50] The presence of the secondary peak at λ'_{max}, however, is unique to the latter process. As d_s decreases, the surface plasmon resonance peak increasingly red-shifts to longer wavelengths (λ_{max}) until it "devolves" into

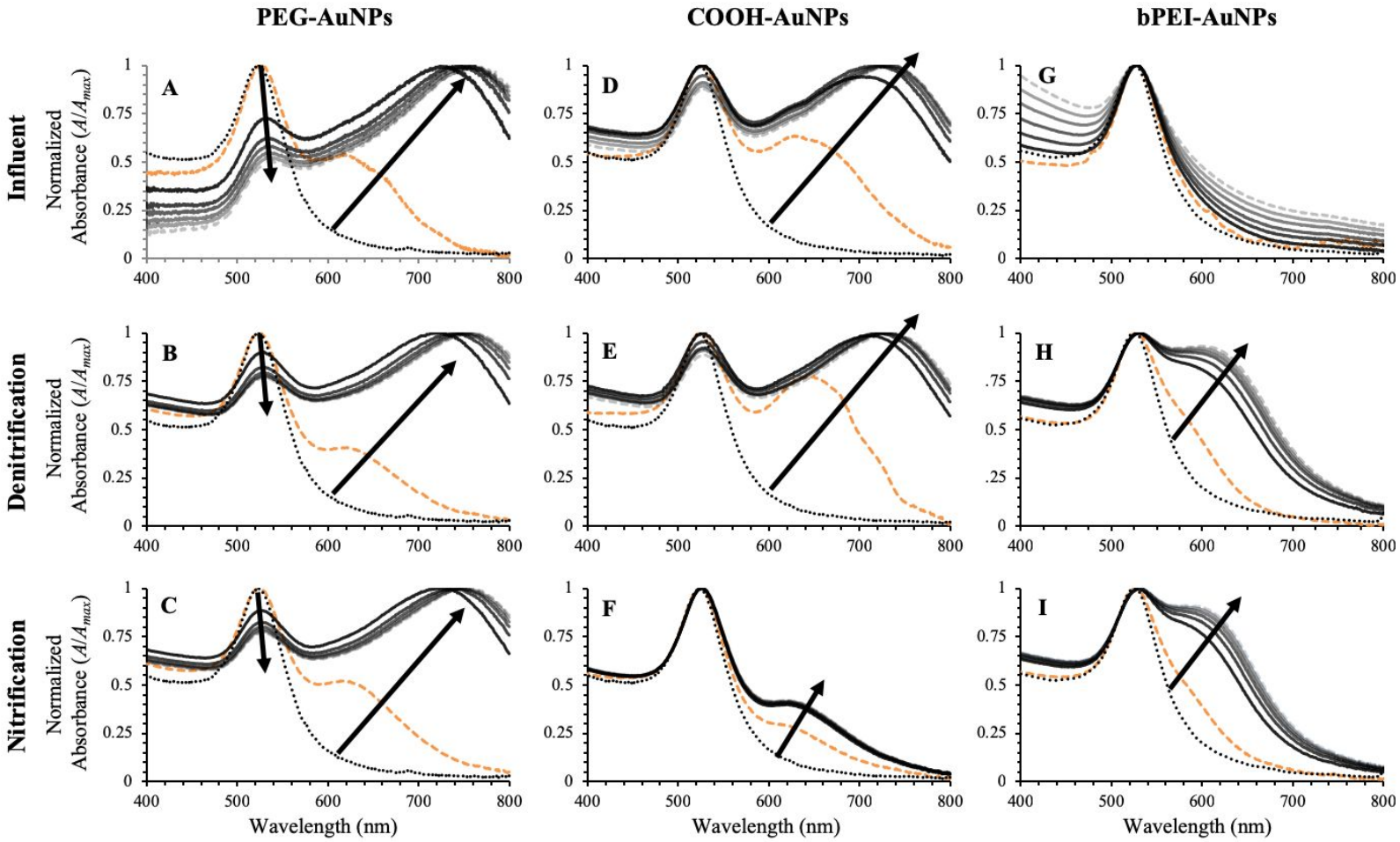

Figure 3. Background-corrected and normalized (A/A_{max}) UV-Vis spectra for (a-c) PEG-AuNPs, (d-f) COOH-AuNPs, and (g-i) bPEI-AuNPs in (top) influent (middle) denitrification and (bottom) nitrification wastewater matrices. Orange dashed-line depicts the UV-Vis spectra collected

immediately upon addition of AuNPs ($t \leq 20$ seconds), grey dashed-line depicts spectra at $t = 120$ minutes, and grey-scale depicts spectra at 20-minutes intervals in between (black-to-grey). For reference, the black dotted-line depicts the UV-Vis spectra in DDI.

two distinct peaks—the transverse surface plasmon resonance peak occurring in proximity to λ_{SPR} (i.e., λ_{max}) and the longitudinal surface plasmon resonance peak found at longer wavelengths (i.e., λ'_{max}).[49] These two distinct peaks are a characteristic feature of anisotropic metallic ENMs with high aspect ratios, such as gold nanorods.[51] With respect to spherical AuNPs, these peaks are a function of the orientation of the incident light path relative to the long-axis of two adjacent AuNPs and d_s.[49,50]

This phenomena was explored by Rechberger et al. (2003)[49] and Sendroiu et al. (2006)[50], who investigated the relation of the spectral aggregation shift ($\Delta\lambda_{agg} = \lambda'_{max} - \lambda_{max}$) to the ratio of d_s to nanoparticle diameter ($d_s/2r_c$) for particle pairs in well-controlled systems. According to Sendroiu et al. (2006)[50], $\Delta\lambda_{agg}$ was found to exponentially increase with decreasing d_s, with $\Delta\lambda_{agg} \approx 100$ nm indicative of $d_s/2r_c \approx 1.0$ for doublets in suspension.[50] In the present study, we find $\Delta\lambda_{agg}$ for the PEG-AuNPs varied between ≈203 nm (nitrification) and ≈225 nm (influent and denitrification). By analyzing the TEM micrographs to measure d_s between neighboring primary particle pairs within each aggregate assemblage and using the reported value of D_c (Table 1), the ratio of $d_s/2r_c$ was calculated (see Supplementary Information for details). For the PEG-AuNPs in each wastewater matrix, $d_s/2r_c$ was consistently ≈1.07 (Table 2), with the primary particles separated by a few nanometers in each aggregate assemblage.

Table 2. Average center-to-center separation distance (d_s) and its ratio to nanoparticle diameter ($d_s/2r_c$) calculated for each AuNP type in each wastewater matrix.

Surface Coating	Core Diameter, D_c (nm)	Influent		Denitrification		Nitrification	
		d_s (nm)	$d_s/2r_c$	d_s (nm)	$d_s/2r_c$	d_s (nm)	$d_s/2r_c$
PEG	40 ± 3	42.6 ± 0.4	1.06 ± 0.01	42.8 ± 0.3	1.07 ± 0.01	42.6 ± 0.2	1.07 ± 0.004
COOH	40 ± 5	41.4 ± 0.7	1.04 ± 0.02	43.2 ± 0.4	1.08 ± 0.01	42.7 ± 0.5	1.07 ± 0.01
bPEI	42 ± 5	44.0 ± 0.6	1.05 ± 0.01	42.8 ± 0.4	1.02 ± 0.01	44.4 ± 0.6	1.06 ± 0.01

Error bars indicate ± 95% confidence interval (*n* varies; see Figures S21 – S23).

The overall TR-UV-Vis and TEM patterns reported herein are in line with the findings observed by Rechberger et al. (2003) and Sendroiu et al. (2006). Our finding that $\Delta\lambda_{agg}$ ≈200 – 225 nm corresponds with $d_s/2r_c$ ≈ 1.07 differs from the results reported previously and is likely an effect of analyzing large aggregate assemblages as opposed to carefully patterned AuNPs fixed on a surface. These differences highlight the limitations of utilizing UV-Vis measurements alone to assess the structure of ENM aggregates in complex matrices. The TEM results, which clearly indicate that the PEG-AuNPs formed large aggregates consisting of primary particles separated by a few nanometers, are consistent with both the TR-DLS measurements and general UV-Vis spectral trends and demonstrate the benefit of using multiple, corroborative techniques.

The UV-Vis results further suggest that as the PEG-AuNPs aggregated, either the structure of PEG surface coating underwent significant conformational changes or an organic matter corona formed via adsorption of organic macromolecules to the surface coating (overcoating) or directly to the AuNP surface (displacement). It is not possible to distinguish between these processes with

the current experimental approach. However, the electrophoretic mobility (EPM) of the PEG-AuNPs measured after incubation in each filtered wastewater matrix was less negative than that measured in the 1 mM NaCl and was comparable across each matrix (Figure 4). Previous research indicates that the background organic matter in wastewater matrices is mainly comprised of extracellular polymeric substances (EPS), which typically possess a negative surface charge due to the presence of various charged functional groups, such as carboxyl, phenolic and hydroxyl groups.[52–54] Based on the UV-Vis results and the trends in the EPM data it is hypothesized that upon dispersion in the wastewater matrices, the PEG-AuNPs acquired a corona comprised of these organic macromolecules from the surrounding matrix. This corona clearly negates the stabilization provided by the PEG coating, allowing the PEG-AuNPs to form closely-spaced particle aggregates.

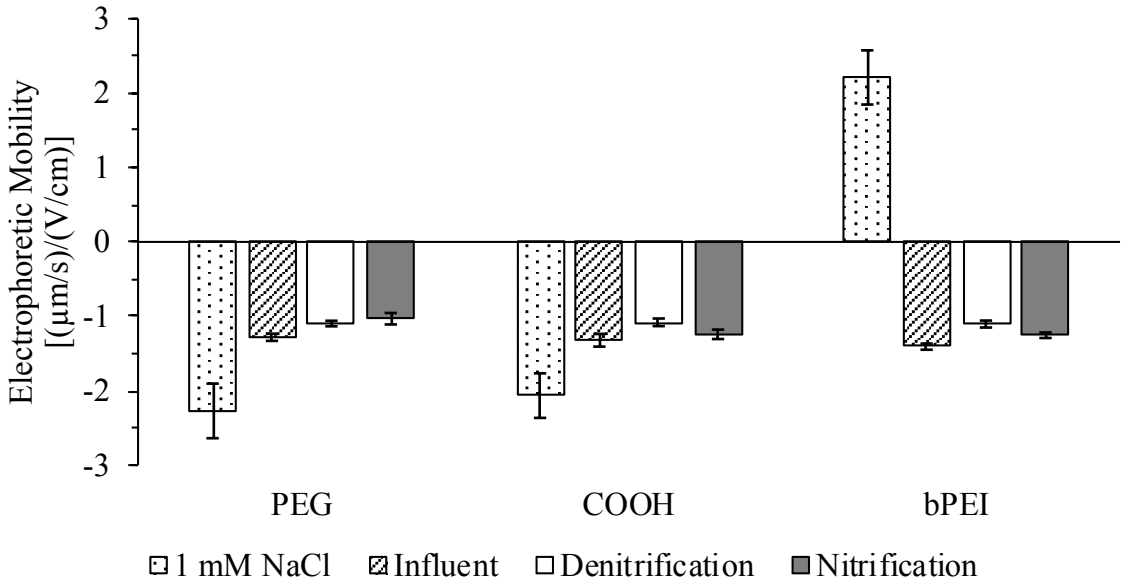

Figure 4: Electrophoretic mobility (EPM) of each AuNP type in each wastewater matrix at pH 8.0 ± 0.04 and in 1 mM NaCl (see Table 1). Error bars indicate ± 95% confidence interval (*n* = 3).

Previous research has demonstrated that the PEG surface coating electrosterically stabilizes the PEG-AuNPs across a range of conditions, including up to very high ionic strengths (up to 1.5 M) and various mass concentration ratios of natural organic matter to AuNPs (i.e. [NOM]:[NP]).[43,44] For the current work, the ionic strength of the wastewater matrices varied between 18.4 – 21.7 mM and [NOM]:[NP] was between 16.4 – 168.0 mg C/mg Au (Table S2). The ionic strength of the wastewater matrices is significantly lower than the conditions of the prior work, indicating that electric double layer (EDL) compression is not a relevant mechanism causing the PEG-AuNPs to aggregate.

While NOM has not been found to affect the aggregation behavior of the PEG-AuNPs, it appears that the organic matter in the wastewater matrices interacts with the PEG-AuNPs differently than NOM from freshwater sources. The composition of organic matter in WWTPs has been found to differ in relation to the aquatic chemistry and microbial community of different WW treatment processes.[52–54] Characterization of the organic matter in the wastewater matrices was beyond the scope of this work. However, previous research has shown that wastewater-derived EPS is predominately comprised of carbohydrates and proteins, although humic substances are also a major component in activated sludge treatment processes.[52–54] For a detailed discussion regarding the composition of EPS in wastewater treatment systems, the reader is referred to the review by Sheng et al. (2010)[52] and the references contained therein. Variations in organic matter composition have been shown to influence the formation of microbial aggregates in wastewater treatment processes, particularly in the presence of divalent cations.[53,55–57] It is hypothesized that

the EPS produced from the microbial communities in the WWTP interacts and alters the aggregation behavior of the PEG-AuNPs differently than freshwater-derived NOM. These interactions may also be facilitated by the presence of high concentrations of divalent cations (Table S2) as well as other solutes not typically found in freshwater environments, such as the nitrogenous species ammonia (NH_4^+), nitrite (NO_2^-) and nitrate (NO_3^-; Table S2). These species could interact with the PEG surface coating through specific interactions (i.e., the terminal hydroxyl [OH] moiety exhibits zwitterionic behavior) or non-specific interactions with the poly(ethylene oxide) chain.[58]

COOH-AuNPs. With some exceptions, similar trends to those noted with the PEG-AuNPs were observed for the COOH-AuNPs. The TR-DLS measurements demonstrate that the COOH-AuNPs aggregated in each wastewater matrix, although $D_{h,final}/D_{h,inital}$ was lower in the influent wastewater compared to the filtered mixed liquor matrices from the activated sludge process (Figure 1 and Figure S7). The TEM micrographs also indicate that the COOH-AuNPs aggregated in each wastewater matrix (Figures 2d-f) but not to the extent observed for the PEG-AuNPs, indicated by the larger number of smaller (<1 µm) aggregates.

Where the COOH- and PEG-AuNPs notably differ is in their respective TR-UV-Vis spectra. With the exception of one replicate (Figure S16), quenching of the primary peak at λ_{max} was not observed for the COOH-AuNPs (background-correct spectrum in Figures S14 – S16). Instead, the peak height at λ_{max} was generally greater at t = 120 minutes than that measured at $t \approx 0$ minutes (Figures S14

– S16), which is attributed to small variations in the background UV-Vis spectra measured in the absence of the AuNPs (Figure S2e). The red-shift at λ_{max} (Figure S10) and the distinct secondary peak at λ'_{max} ≈ 740 nm (Figures 3d-e), were observed for the COOH-AuNPs in the influent and denitrification wastewater matrices, although the red-shift was not statistically significant in the influent wastewater matrix. In the nitrification wastewater matrix, the red-shift at λ_{max} was less pronounced than that observed in the denitrification matrix (Figure S10) while the secondary peak at λ'_{max} occurs at a shorter wavelength (λ'_{max} ≈ 630 nm) and reaches a lower absorbance compared to λ_{max} (Figure 3f), resembling the "shoulder" observed in the initial PEG-AuNP TR-UV-Vis spectra.

These differences suggest that the structure of the COOH-AuNP aggregates formed in each matrix was slightly different. The $\Delta\lambda_{agg}$ was much lower in the nitrification wastewater (≈106 nm) compared to the influent and denitrification wastewater matrices (≈206 and ≈211 nm, respectively). Based on the trends previously reported[49,50], the TR-UV-Vis data suggests that d_s between adjacent COOH-AuNPs would be greater in the nitrification wastewater than the influent or denitrification wastewater. However, analysis of the TEM micrographs reveal that d_s was lowest in the influent wastewater matrix and was comparable in the denitrification and nitrification wastewater matrices (Table 2). As noted previously, the divergence between the UV-Vis and TEM measurements likely reflects the heterogeneous nature of the aggregates formed. Overall, the finding that $d_s/2r_c$ in the various matrices was ≈1.04 – 1.08 reveals that the COOH-AuNPs, like the PEG-AuNPs, formed aggregates containing closely-spaced primary particles separated by a few nanometers.

With similar trends as the PEG-AuNPs, UV-vis and EPM data (Figures 3 and 4) suggest that the COOH-AuNPs also acquire a corona of organic macromolecules via specific interactions with the carboxylic (COOH) moiety or non-specific interactions with the poly(ethylene oxide) chain. The relatively higher $d_s/2r_c$ in the denitrification and nitrification wastewater matrices may indicate that the composition of this corona is different than those formed on the COOH-AuNPs dispersed in the influent wastewater matrix. As such, the combination of varying organic matter composition and aquatic chemistry may have altered the aggregation behavior and the resulting aggregate structure of the COOH-AuNPs in each wastewater treatment stage.

bPEI-AuNPs. The bPEI-AuNPs experienced different extents of aggregation in the three matrices; $D_{h,final}/D_{h,initial}$ was lowest in the influent matrix and highest in the nitrification matrix (Figure 1). A distinct feature observed during the bPEI-AuNP TR-DLS measurements was a near-instantaneous increase in D_h of ≈20 – 30 nm that was common across the wastewater matrices (Figure S8). After this initial increase in D_h, the bPEI-AuNPs appear resistant to further aggregation in the influent wastewater matrix. However, TR-DLS measurements performed over a much longer time period reveal that after ≈50 minutes (coinciding with the end of the 'shorter' TR-DLS measurement period), the bPEI-AuNPs begin to aggregate in the influent matrix (Figure S9). After ≈120 minutes, the D_h of the bPEI-AuNPs approaches 200 nm and was comparable to that measured for the PEG-AuNPs over the same period. In general, the TEM micrographs support the finding that the bPEI-AuNPs were physically transformed via aggregation (Figures 2g-i). In all three wastewater

matrices, the bPEI-AuNPs formed some large aggregates (Figures 2g-i), although a considerable amount of smaller aggregates (e.g., dimers and trimers) formed in the influent wastewater matrix.

The TR-UV-Vis spectra obtained with the bPEI-AuNPs has some similarities to those obtained with the PEG- and COOH-AuNPs. Like the COOH-AuNPs, the peak height at λ_{max} was consistently greater at t = 120 minutes versus t ≈0 minutes (background-corrected spectrum in Figures S17 – S19), which we again attribute to small variations in the background UV-Vis spectra measured in the absence of the AuNPs (Figure S2e). In addition, as was observed with the PEG- and COOH-AuNPs, λ_{max} was red-shifted relative to λ_{SPR} (Figure S10). Unlike the PEG- and COOH-AuNPs, however, no secondary peak was noted when the bPEI-AuNPs were dispersed in the influent wastewater matrix (Figure 3g). In the denitrification and nitrification wastewater matrices, a "shoulder" at λ'_{max} ≈ 600 nm consistently appeared at a slightly lower peak height compared to λ_{max} (Figures 3h-i and Figures S18 – S19). Compared to the PEG- and COOH-AuNPs, $\Delta\lambda_{agg}$ was much lower in the denitrification and nitrification wastewater matrices (≈71 nm) and negligible in the influent wastewater matrix. However, analysis of the TEM micrographs reveals that $d_s/2r_c$ for the bPEI-AuNPs was comparable to the other AuNP types (Table 2).

For the bPEI-AuNPs, there is a clear indication that the surface coatings underwent charge reversal in each wastewater matrix, changing from highly positive in the 1 mM NaCl to negative in all three wastewater matrices (Figure 4). In combination with the near-instantaneous increase in D_h observed via TR-DLS (Figure S8) and the features observed during the TR-UV-Vis measurements

(Figures 3g-i), it can be inferred that the bPEI-AuNPs acquired a corona from the surrounding wastewater matrices. It is hypothesized that the corona acquired by the bPEI-AuNPs occurred through adsorption of the organic macromolecules to the amine moieties. Given the initial positive charge of the bPEI-AuNPs, this coating would favor interactions with the negatively-charged organic macromolecules that are ubiquitous in wastewater matrices.[52–54] This behavior has been observed previously in simulated and real freshwater media when NOM was present.[43,44] In the simulated freshwater medium at pH 8.0 (comparable to the pH of the wastewater matrices [Table S2]), it was found that [NOM]:[NP] ≥ ≈0.3 mg C/mg Au resulted in charge reversal of the bPEI-AuNPs via NOM adsorption.[43] Based on this, it is expected that the [NOM]:[NP] in the current work, which varied between 16.4 – 168.0 mg C/mg Au (Table S2), would result in an organic matter corona extensively overcoating the bPEI-AuNPs. This hypothesis is also supported by the spectral trends (e.g., red-shift) in the TR-UV-Vis data at λ_{max} (Figures 3g-i and S10). Like the other AuNPs investigated, the bPEI-AuNPs aggregated upon dispersion in the wastewater matrices, mostly likely via the formation of an organic matter corona and interparticle bridging similar to previous observations.

Summary. Each AuNP type underwent somewhat different transformations in each of the wastewater matrices; yet, several overarching trends were observed. First, all three AuNPs types were found to aggregate, which we hypothesize is linked to the corona they acquired upon dispersion in the wastewater matrices. Evidence that the AuNPs acquired an organic matter corona is based on the features observed during the TR-UV-Vis measurements and the finding

that the EPM of each AuNP type was comparable in the three wastewater matrices (Figure 4). For the bPEI-AuNPs, reversal of the surface charge was a clear indicator that organic macromolecules had adsorbed and facilitated aggregation.[43,44] The mechanisms resulting in the formation of an organic matter corona on the PEG- and COOH-AuNPs are not clear. However, their formation may have been influenced by the nature of the organic matter and the high concentration of divalent cations and other solutes in the wastewater matrices (Table S2) that are not common in natural freshwater environments. Previous work with the same nanoparticle types indicate that the PEG and COOH-AuNPs are not destabilized by charge screening or charge neutralization,[43,44] suggesting that specific interactions between components of the wastewater organic matter and the engineered surface coatings (e.g. bridging) are facilitating aggregation. It is hypothesized that variations in the composition of the corona layer formed on the AuNPs affected the structure (i.e., center-to-center separation distance) of the ENM aggregates that formed in each of the wastewater matrices.

Second, the timescale of the transformations was on the order of seconds-to-minutes. For the PEG- and COOH-AuNPs, changeds in the UV-Vis spectra (e.g., presence of secondary peak at λ'_{max}) are first evident during the initial measurement immediately following the addition of the AuNPs to the wastewater matrices (estimated to be ≤ 20 seconds). For the bPEI-AuNPs, changes in the UV-Vis spectra are also initially apparent but were more pronounced by the second measurement at t = 20 minutes, while an initial increase in D_h during the TR-DLS measurements was noted within the first minute.

Transformations during Changing Wastewater Matrices

Batch Experiments vs. Baseline Matrix Exchange. For each AuNP type, the $D_{h,final}/D_{h,initial}$ calculated during the baseline matrix exchange procedure after ≈45 minutes is slightly higher than that measured during the batch experiments over the same period of time (Figure 5). This is attributed to increased particle-particle collisions via fluid shear occurring in the TFF system, which were absent in the batch measurements. Nonetheless, the relative trend in $D_{h,final}/D_{h,initial}$ between the two methods is comparable, with PEG > COOH ≈ bPEI.

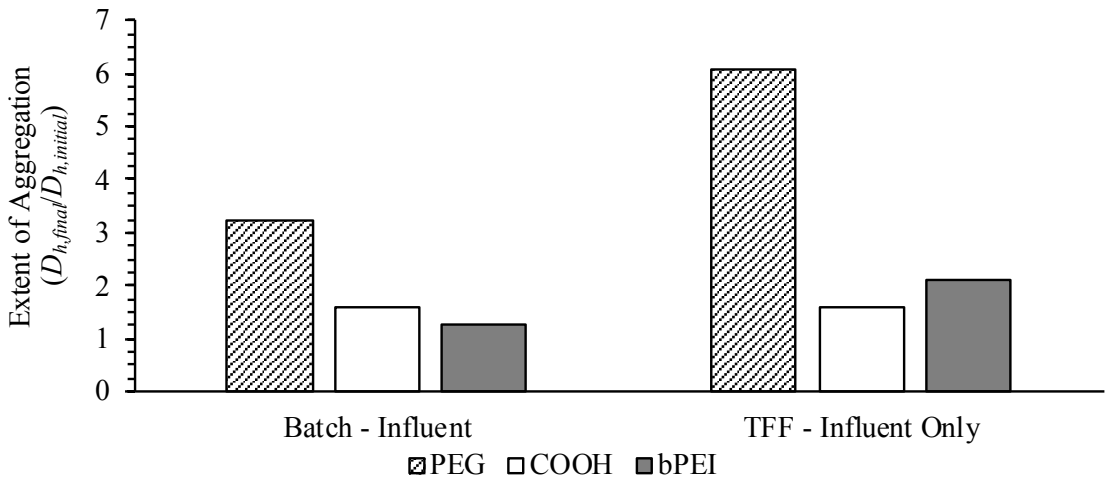

Figure 5. Extent of aggregation ($D_{h,final}/D_{h,initial}$) of each AuNP type during (left) batch experiments and (right) the wastewater matrix exchange procedure with only the influent wastewater matrix after ≈45 minutes.

During the baseline matrix exchange procedure, the UV-Vis spectra recorded for the PEG-AuNPs indicates the presence of two peaks, one in proximity to λ_{SPR} (i.e., λ_{max}) and another at $\lambda \approx 725$ nm (λ'_{max}, Figure 6a). The signal attributed to the PEG-AuNPs is obscured by the background wastewater matrix at $t \geq 60$ min., indicated by the highest absorbance at $\lambda \leq 400$ nm that gradually decreases as λ increases. This indicates that over time the signal attributable to the PEG-AuNPs is lost, which could be from the loss of the PEG-AuNPs via attachment to the PES membrane or from their aggregation and subsequent extraction within the retentate for DLS and UV-Vis analysis. The UV-Vis spectra for the COOH-AuNPs measured during the baseline matrix exchange procedure has similar features to those observed with the PEG-AuNPs. Initially, only a single peak is evident at λ_{max} but over time a secondary peak appears (λ'_{max}, Figure 6c), initially at $\lambda'_{max} \approx 630$ nm before red-shifting to $\lambda'_{max} \approx 680$ nm. Unlike the PEG- and COOH-AuNPs, only a single peak is evident in the bPEI-AuNP UV-Vis spectra (Figure 6e), consistently appearing in proximity to λ_{SPR}. As with the

DLS data, the relative trends in the UV-Vis spectra for each AuNP type during the baseline matrix exchange procedure are comparable to those observed during the batch experiments using the influent wastewater matrix. These features include the secondary peak at λ'_{max} for the PEG- (Figures 3a and 6a) and COOH-AuNPs (Figures 3d and 6c) and the absence of secondary peak at λ'_{max} for the bPEI-AuNPs (Figures 3g and 6e).

In general, the similarity in the trends observed with the two methods indicates that the transformations occurring to the AuNPs during the two experimental methods are comparable. From this, we can assess how changing the background wastewater matrix affects the transformations occurring to the AuNPs by comparing the results to those obtained during the batch measurements.

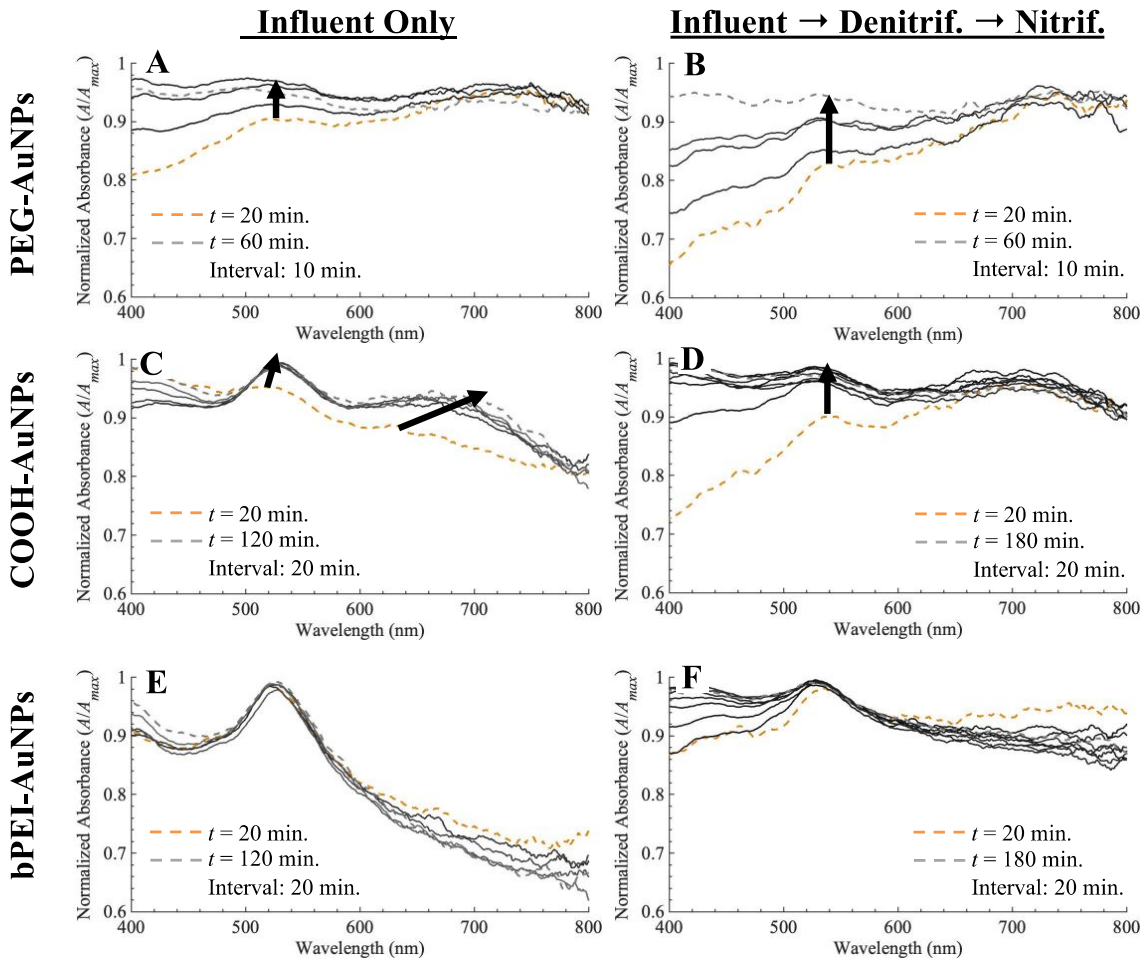

Figure 6. Background-corrected and normalized (A/A_{max}) UV-Vis spectra for (a,b) PEG-AuNPs, (c,d) COOH-AuNPs, and (e,f) bPEI-AuNPs during wastewater matrix exchange testing.

Baseline vs. Double Matrix Exchange. The extent of aggregation ($D_{h,final}/D_{h,initial}$) calculated for each AuNP type after ≈120 minutes exposure to only the influent wastewater (baseline) and after sequential exposure to the influent, denitrification, and nitrification matrices (double matrix exchange) are shown in Figure 7. During both experiments, the trends in $D_{h,final}/D_{h,initial}$ were the same and comparable to those observed during the batch experiments (Figure 1), with PEG > COOH ≈ bPEI. The D_h of the PEG-AuNPs increased to ≈390 nm and ≈590 nm (baseline and double

matrix exchange, respectively). In contrast, the D_h of the COOH-AuNPs only increased to ≈125 nm and ≈320 nm while D_h of the bPEI-AuNPs increased to ≈100 nm and ≈230 nm (baseline and double matrix exchange, respectively). These trends were confirmed via TEM, which indicated the presence of few but large PEG-AuNP aggregates upwards of 1 µm, a large number of moderately-sized COOH-AuNPs aggregates, and many lower-order bPEI-AuNP aggregates, such as dimers and trimers (Figure S24).

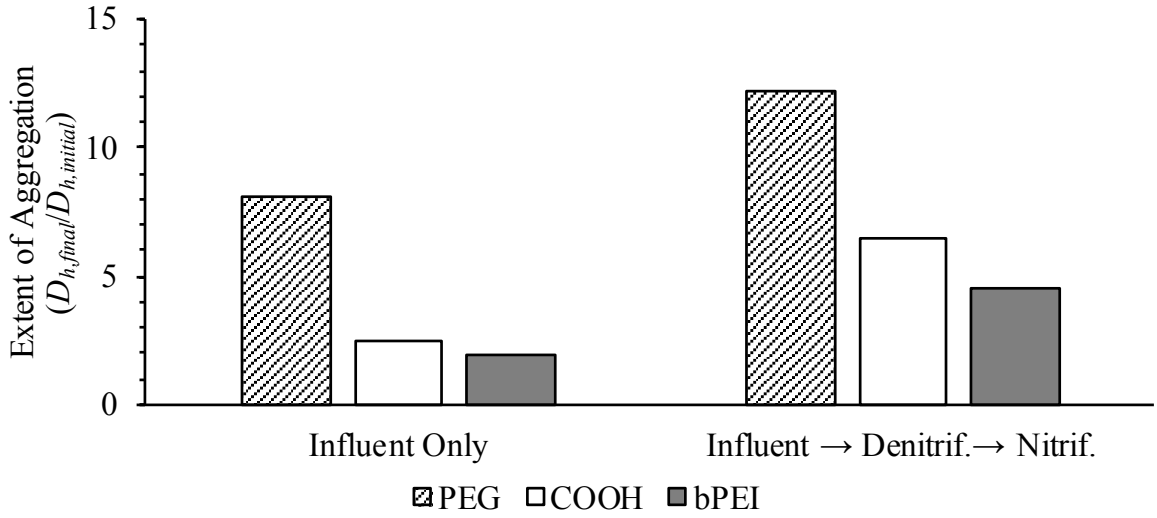

Figure 7. Extent of aggregation ($D_{h,final}/D_{h,initial}$) of each AuNP type during the wastewater matrix exchange procedure after ≈120 minutes.

The higher $D_{h,final}/D_{h,initial}$ observed during the double matrix exchange experiments may reflect changes in the composition of the background matrix. During the batch measurements, $D_{h,final}/D_{h,initial}$ of the COOH- and bPEI-AuNPs was greater in both the denitrification and nitrification wastewater matrices relative to that measured in the influent wastewater matrix (Figure 1). However, this behavior was not observed with the PEG-AuNPs, which aggregated to similar

extents in each of the wastewater matrices during the batch experiments (Figure 1). Nonetheless, the increased $D_{h,final}/D_{h,initial}$ during the double matrix exchange experiments suggests that changing the composition of the background matrix may influence the aggregation behavior of the AuNPs. It may have been that the AuNPs, after initially acquiring an organic matter corona from the influent wastewater matrix, continued aggregating due to the presence of some constituent that was absent from the influent wastewater matrix. This may reflect changes in the aquatic chemistry within each of the wastewater matrices, such as the reduction-oxidation reactions that change the relative amounts of the nitrogenous species ammonia (NH_4^+), nitrite (NO_2^-) and nitrate (NO_3^-) between each of the wastewater treatment stages

The TR-UV-Vis spectra measured for each AuNP type during the double matrix exchange experiments are also shown in Figure 6. In general, the spectral patterns mimic those obtained during the baseline matrix exchange experiment. The location of secondary peaks for the PEG- and COOH-AuNPs were found at comparable wavelengths as those during the baseline measurements. Likewise, only a single peak in proximity to λ_{SPR} was observed for the bPEI-AuNPs during the double matrix exchange experiment. The similarity in the UV-Vis spectra between the baseline and double matrix exchange procedures for all the AuNPs reveals that similar transformations to the AuNPs are likely occurring, even as the background matrix changes. Stated another way, these results indicate that the initial transformations occurring to the AuNPs upon their exposure to the influent matrix, which are specific to the engineered surface coating, continue to persist even as the composition of the background matrix changes to that of the

subsequent biological treatment stages. The formation of a persistent organic matter corona would have been promoted by the relatively higher amount of organic matter in the influent wastewater ([NOM]:[NP] = 168 mg C/mg Au) compared to that of the biological treatment stages ([NOM]:[NP] =16.4 and 45.9 mg C/mg Au, respectively; Table S2). As with the batch experiments, the mechanisms behind the transformations of the AuNPs appear to be influenced by their initial engineered surface coating. However, all the AuNP types aggregated, probably facilitated by the acquisition of an organic matter corona. As noted previously, the aggregation behavior of the PEG- and COOH-AuNPs was unaffected by the presence of organic matter in simulated and actual freshwater media.[43,44] The results reported herein indicate that the composition and properties of the organic matter within the wastewater matrices was able to interact with and destabilize each of the model AuNPs investigated. This process may have been facilitated by the aquatic chemistry of the wastewater media, which is substantially different than that of freshwater environments.

Implications for Modelling ENM Environmental Fate

Our results highlight the importance of colloid surface properties in influencing the aggregation of ENMs and the formation of organic matter coronas. Furthermore, our results challenge approaches which model environmental fate and exposure to ENMs on the basis of their pristine properties. Each type of the model ENMs investigated underwent transformations when exposed to the wastewater matrices that were specific to the matrix and the initial surface coating of the ENMs. The interaction of the surface coating with constituents in the surrounding matrix altered

ENM aggregation and affected the structure of the aggregates. Furthermore, these transformations occurred over timescales of seconds-to-minutes. In a moderate-sized city (e.g., Zürich, Switzerland), the average residence time for untreated wastewater to reach a treatment facility and the hydraulic residence time (HRT) within a typical wastewater treatment plant (WWTP) are each on the order of several hours.[59,60] Thus, ENMs discharged to surface waters via WWTPs will not retain their initial, pristine properties and will differ from their "engineered" analogs. Finally, the transformations that occurred to the model ENMs during their exposure to the influent wastewater, which are expected to occur as ENMs are transported in sewer systems en route to a treatment facility, persisted even as the background matrix changed.

Recognizing that a majority of ENMs entering WWTPs are removed via aggregation with suspended particulate matter, it is hypothesized that the fraction of ENMs not removed and discharged to surface waters will most likely be present in aggregates >100 nm and possess an organic corona composed of exudates from the microbial community in raw wastewater. In combination, these findings complicate attempts to link the physiochemical properties of pristine ENMs to the processes affecting their environmental fate. Instead, the properties of the ENMs after 'aging' will dictate their environmental fate and will be relevant for accurate exposure assessments. To investigate this further, additional work is aimed at comparing the aggregation behavior of aged ENMs versus their pristine counterparts upon dispersion in samples from a natural, freshwater river. Furthermore, the nature of the corona acquired by the model ENMs used in the current study will be further investigated via surface sensitive techniques to explore

the kinetics of organic matter adsorption, the mechanisms of corona formation and the composition/structure of the adsorbed layer.

ELECTRONIC SUPPLEMENTARY INFORMATION

Electronic Supplementary Information (ESI) available, including: characterization of the model ENMs and wastewater matrices, the replicate TR-DLS and UV-Vis measurements, details of the UV-Vis data handling and TEM analysis, and ancillary tests performed to support the experimental design.

AUTHOR INFORMATION

Corresponding Authors:

[§] Email: Jeff.Nason@oregonstate.edu Phone: +1 541 737 9911

[*] Email: Ralf.Kaegi@eawag.ch Phone: +41 058 765 52 73

CONFLICTS OF INTEREST

There are no conflicts of interest to declare.

ACKNOWLEDGEMENTS

This research was supported by the National Science Foundation (NSF) Graduate Research Fellowship Program under Grant No. DGE-1314109 and NSF Grant No. 1255020, and through the NSF Graduate Research Opportunities Worldwide (GROW) Program. Any opinions, findings, and conclusions or recommendations expressed in this material are those of the author(s) and do not necessarily reflect the views of the NSF. Additional support was provided by the Swiss National Science Foundation (SNF) under Project No. 177090. We acknowledge the Scientific Center for Optical and Electron Microscopy (ScopeM) of the ETH Zürich for providing access to their microscopes. Special thanks to B. Sinnet for assistance throughout the project, J. Traber for assistance with the TFF system, and D. Mitrano for suggestions during the experimental design.

REFERENCES

1 H. H. Liu and Y. Cohen, Multimedia environmental distribution of engineered nanomaterials, *Environ. Sci. Technol.*, 2014, **48**, 3281–3292.

2 J. Meesters, A. A. Koelmans, J. T. K. Quik, A. J. Hendriks and D. Van De Meent, Multimedia modeling of engineered nanoparticles with simpleBox4nano: Model definition and evaluation, *Environ. Sci. Technol.*, 2014, **48**, 5726–5736.

3 K. L. Garner, S. Suh and A. A. Keller, Assessing the Risk of Engineered Nanomaterials in the Environment: Development and Application of the nanoFate Model, *Environ. Sci. Technol.*, 2017, **51**, 5541–5551.

4 A. L. Dale, E. A. Casman, G. V. Lowry, J. R. Lead, E. Viparelli and M. Baalousha, Modeling Nanomaterial Environmental Fate in Aquatic Systems, *Environ. Sci. Technol.*, 2015, **49**, 2587–2593.

5 G. Raza, M. Amjad, I. Kaur, M. Baalousha, J. R. Lead and D. Wen, Stability and Aggregation Kinetics of Titania Nanomaterials under Environmentally Realistic Conditions, *Environ. Sci. Technol.*, 2016, **50**, 12525–12525.

6 A. Praetorius, R. Arvidsson, S. Molander and M. Scheringer, Facing complexity through informed simplifications: a research agenda for aquatic exposure assessment of

nanoparticles, *Environ. Sci. Process. Impacts*, 2013, **15**, 161–168.

7 U. Weilenmann, C. R. O'Melia and W. Stumm, Particle transport in lakes: Models and measurements, *Limnol. Oceanogr.*, 1989, **34**, 1–18.

8 J. Buffle and G. G. Leppard, Characterization of Aquatic Colloids and Macromolecules. 1. Structure and Behavior of Colloidal Material, *Environ. Sci. Technol.*, 1995, **29**, 2169–2175.

9 J. Buffle, K. J. Wilkinson, S. Stoll, M. Filella and J. Zhang, A Generalized Description of Aquatic Colloidal Interactions: The Three-colloidal Component Approach, *Environ. Sci. Technol.*, 1998, **32**, 2887–2899.

10 G. V. Lowry, K. B. Gregory, S. C. Apte and J. R. Lead, Transformations of Nanomaterials in the Environment, *Environ. Sci. Technol.*, 2012, **46**, 6893–6899.

11 A. Praetorius, J. Labille, M. Scheringer, A. Thill, K. Hungerbühler and J. Bottero, Heteroaggregation of Titanium Dioxide Nanoparticles with Model Natural Colloids under Environmentally Relevant Conditions, *Environ. Sci. Technol.*, 2014, **48**, 10690–10698.

12 L. E. Barton, M. Therezien, M. Auffan, J.-Y. Bottero and M. R. Wiesner, Theory and Methodology for Determining Nanoparticle Affinity for Heteroaggregation in Environmental Matrices Using Batch Measurements, *Environ. Eng. Sci.*, 2014, **31**, 421–427.

13 N. K. Geitner, N. J. O'Brien, A. A. Turner, E. J. Cummins and M. R. Wiesner, Measuring Nanoparticle Attachment Efficiency in Complex Systems, *Environ. Sci. Technol.*, 2017, **51**, 13288–13294.

14 J. A. Gallego-Urrea, J. Hammes, G. Cornelis and M. Hassellöv, Coagulation and sedimentation of gold nanoparticles and illite in model natural waters: Influence of initial particle concentration, *NanoImpact*, 2016, **3–4**, 67–74.

15 G. V. Lowry, B. P. Espinasse, A. R. Badireddy, C. J. Richardson, B. C. Reinsch, L. D. Bryant, A. J. Bone, A. Deonarine, S. Chae, M. Therezien, B. P. Colman, H. Hsu-Kim, E. S. Bernhardt, C. W. Matson and M. R. Wiesner, Long-Term Transformation and Fate of Manufactured Ag Nanoparticles in a Simulated Large Scale Freshwater Emergent Wetland, *Environ. Sci. Technol.*, 2012, **46**, 7027–7036.

16 A. L. Dale, G. V. Lowry and E. A. Casman, Modeling Nanosilver Transformations in Freshwater Sediments, *Environ. Sci. Technol.*, 2013, **47**, 12920–12928.

17 X. Feng, Y. Yan, B. Wan, W. Li, D. P. Jaisi, L. Zheng, J. Zhang and F. Liu, Enhanced Dissolution and Transformation of ZnO Nanoparticles: The Role of Inositol Hexakisphosphate, *Environ. Sci. Technol.*, 2016, **50**, 5651–5660.

18 S. M. Louie, R. D. Tilton and G. V. Lowry, Critical review: impacts of macromolecular coatings on critical physicochemical processes controlling environmental fate of

nanomaterials, *Environ. Sci. Nano*, 2016, **3**, 283–310.

19 S. M. Louie, R. D. Tilton and G. V. Lowry, Effects of molecular weight distribution and chemical properties of natural organic matter on gold nanoparticle aggregation., *Environ. Sci. Technol.*, 2013, **47**, 4245–54.

20 S. Jayalath, S. C. Larsen and V. H. Grassian, Surface adsorption of Nordic aquatic fulvic acid on amine-functionalized and non-functionalized mesoporous silica nanoparticles, *Environ. Sci. Nano*, 2018, **5**, 2162–2171.

21 A. A. Keller, S. McFerran, A. Lazareva and S. Suh, Global life cycle releases of engineered nanomaterials, *J. Nanoparticle Res.*, 2013, **15**, 1692.

22 A. A. Keller, W. Vosti, H. Wang and A. Lazareva, Release of engineered nanomaterials from personal care products throughout their life cycle, *J. Nanoparticle Res.*, 2014, **16**, 2489.

23 T. Y. Sun, N. A. Bornhöft, K. Hungerbühler and B. Nowack, Dynamic Probabilistic Modeling of Environmental Emissions of Engineered Nanomaterials, *Environ. Sci. Technol.*, 2016, **50**, 4701–4711.

24 F. Gottschalk, T. Y. Sun and B. Nowack, Environmental concentrations of engineered nanomaterials: Review of modeling and analytical studies, *Environ. Pollut.*, 2013, **181**, 287–300.

25 N. C. Mueller and B. Nowack, Exposure Modeling of Engineered Nanoparticles in the Environment, *Environ. Sci. Technol.*, 2008, **42**, 4447–4453.

26 T. Yin, F. Gottschalk, K. Hungerbühler and B. Nowack, Comprehensive probabilistic modelling of environmental emissions of engineered nanomaterials, *Environ. Pollut.*, 2014, **185**, 69–76.

27 N. A. Bornhöft, T. Y. Sun, L. M. Hilty and B. Nowack, A dynamic probabilistic material flow modeling method, *Environ. Model. Softw.*, 2016, **76**, 69–80.

28 T. Y. Sun, D. M. Mitrano, N. A. Bornhöft, M. Scheringer, K. Hungerbühler and B. Nowack, Envisioning Nano Release Dynamics in a Changing World: Using Dynamic Probabilistic Modeling to Assess Future Environmental Emissions of Engineered Nanomaterials, *Environ. Sci. Technol.*, 2017, **51**, 2854–2863.

29 A. Lazareva and A. A. Keller, Estimating potential life cycle releases of engineered nanomaterials from wastewater treatment plants, *ACS Sustain. Chem. Eng.*, 2014, **2**, 1656–1665.

30 R. Kägi, A. Voegelin, C. Ort, B. Sinnet, B. Thalmann, J. Krismer, H. Hagendorfer, M. Elumelu and E. Mueller, Fate and transformation of silver nanoparticles in urban wastewater systems, *Water Res.*, 2013, **47**, 3866–3877.

31 M. A. Kiser, H. Ryu, H. Jang, K. Hristovski and P. Westerhoff, Biosorption of nanoparticles to heterotrophic wastewater biomass, *Water Res.*, 2010, **44**, 4105–4114.

32 R. Kägi, A. Voegelin, B. Sinnet, S. Zuleeg, H. Hagendorfer, M. Burkhardt and H. Siegrist, Behavior of Metallic Silver Nanoparticles in a Pilot Wastewater Treatment Plant, *Environ. Sci. Technol.*, 2011, **45**, 3902–3908.

33 B. Kim, C.-S. Park, M. Murayama and M. F. Hochella, Discovery and Characterization of Silver Sulfide Nanoparticles in Final Sewage Sludge Products, *Environ. Sci. Technol.*, 2010, **44**, 7509–7514.

34 L. Li, M. Stoiber, A. Wimmer, Z. Xu, C. Lindenblatt, B. Helmreich and M. Schuster, To What Extent Can Full-Scale Wastewater Treatment Plant Effluent Influence the Occurrence of Silver-Based Nanoparticles in Surface Waters?, *Environ. Sci. Technol.*, 2016, **50**, 6327–6333.

35 M. A. Kiser, P. Westerhoff, T. Benn, Y. Wang, J. Pérez-Rivera and K. Hristovski, Titanium nanomaterial removal and release from wastewater treatment plants, *Environ. Sci. Technol.*, 2009, **43**, 6757–6763.

36 P. Westerhoff, G. Song, K. Hristovski and M. A. Kiser, Occurrence and removal of titanium at full scale wastewater treatment plants: Implications for TiO2 nanomaterials, *J. Environ. Monit.*, 2011, **13**, 1195–1203.

37 L. K. Limbach, R. Bereiter, E. Muller, R. Krebs, R. Galli and W. J. Srtark, Removal of Oxide Nanoparticles in a Model Wastewater Treatment Plant: Influence of Agglomeration and Surfactants on Clearing Efficiency, *Enviromental Sci. Technol.*, 2008, **42**, 5828–5833.

38 H. P. Jarvie, H. Al-Obaidi, S. M. King, M. J. Bowes, M. J. Lawrence, A. F. Drake, M. A. Green and P. J. Dobson, Fate of silica nanoparticles in simulated primary wastewater treatment, *Environ. Sci. Technol.*, 2009, **43**, 8622–8628.

39 L. Otero-González, J. A. Field, I. A. C. Calderon, C. A. Aspinwall, F. Shadman, C. Zeng and R. Sierra-Alvarez, Fate of fluorescent core-shell silica nanoparticles during simulated secondary wastewater treatment, *Water Res.*, 2015, **77**, 170–178.

40 B. Salieri, D. A. Turner, B. Nowack and R. Hischier, Life cycle assessment of manufactured nanomaterials: Where are we?, *NanoImpact*, 2018, **10**, 108–120.

41 V. Adam, A. Caballero-Guzman and B. Nowack, Considering the forms of released engineered nanomaterials in probabilistic material flow analysis, *Environ. Pollut.*, 2018, **243**, 17–27.

42 D. P. Stankus, S. E. Lohse, J. E. Hutchison and J. A. Nason, Interactions between Natural Organic Matter and Gold Nanoparticles Stabilized with Different Organic Capping Agents, *Environ. Sci. Technol.*, 2011, **45**, 3238–3244.

43 M. C. Surette and J. A. Nason, Effects of surface coating character and interactions with natural organic matter on the colloidal stability of gold nanoparticles, *Environ. Sci. Nano*, 2016, **3**, 1144–1152.

44 M. C. Surette and J. A. Nason, Nanoparticle aggregation in a freshwater river: the role of engineered surface coatings, *Environ. Sci. Nano*, 2019, **6**, 540–553.

45 H. Holthoff, S. U. Egelhaaf, M. Borkovec, P. Schurtenberger and H. Sticher, Coagulation Rate Measurements of Colloidal Particles by Simultaneous Static and Dynamic Light Scattering, *Langmuir*, 1996, **12**, 5541–5549.

46 S. Diegoli, A. L. Manciulea, S. Begum, I. P. Jones, J. R. Lead and J. A. Preece, Interaction between manufactured gold nanoparticles and naturally occurring organic macromolecules, *Sci. Total Environ.*, 2008, **402**, 51–61.

47 V. L. Pallem, H. A. Stretz and M. J. M. Wells, Evaluating Aggregation of Gold Nanoparticles and Humic Substances Using Fluorescence Spectroscopy, *Environ. Sci. Technol.*, 2009, **43**, 7531–7535.

48 F. Frederix, J.-M. Friedt, K.-H. Choi, W. Laureyn, A. Campitelli, D. Mondelaers, G. Maes and G. Borghs, Biosensing Based on Light Absorption of Nanoscaled Gold and Silver Particles, *Anal. Chem.*, 2003, **75**, 6894–6900.

49 W. Rechberger, A. Hohenau, A. Leitner, J. R. Krenn, B. Lamprecht and F. R. Aussenegg, Optical properties of two interacting gold nanoparticles, *Opt. Commun.*, 2003, **220**, 137–141.

50 I. E. Sendroiu, S. F. L. L. Mertens and D. J. Schiffrin, Plasmon interactions between gold nanoparticles in aqueous solution with controlled spatial separation, *Phys. Chem. Chem. Phys.*, 2006, **8**, 1430.

51 C. J. Murphy, T. K. Sau, A. M. Gole, C. J. Orendorff, J. Gao, L. Gou, S. E. Hunyadi and T. Li, Anisotropic metal nanoparticles: Synthesis, assembly, and optical applications, *J. Phys. Chem. B*, 2005, **109**, 13857–13870.

52 G.-P. Sheng, H.-Q. Yu and X.-Y. Li, Extracellular polymeric substances (EPS) of microbial aggregates in biological wastewater treatment systems: A review, *Biotechnol. Adv.*, 2010, **28**, 882–894.

53 M. F. Dignac, V. Urbain, D. Rybacki, A. Bruchet, D. Snidaro and P. Scribe, Chemical Description of Extracellular Polymers: Implications on Activated Sludge Floc Structure, *Water Sci. Technol.*, 1998, **38**, 45–53.

54 J. Zeng, J. M. Gao, Y. P. Chen, P. Yan, Y. Dong, Y. Shen, J. S. Guo, N. Zeng and P. Zhang, Composition and aggregation of extracellular polymeric substances (EPS) in hyperhaline and municipal wastewater treatment plants, *Sci. Rep.*, 2016, **6**, 1–9.

55 M. Esparza-Soto and P. Westerhoff, Biosorption of humic and fulvic acids to live activated sludge biomass, *Water Res.*, 2003, **37**, 2301–2310.

56 X.-M. Liu, H.-W. Luo, F. Zhang, S.-J. Yuan, J. Xu, J.-G. Wu and H.-Q. Yu, Contribution of Extracellular Polymeric Substances (EPS) to the Sludge Aggregation, *Environ. Sci. Technol.*, 2010, **44**, 4355–4360.

57 D. C. Sobeck and M. J. Higgins, Examination of three theories for mechanisms of cation-induced bioflocculation, *Water Res.*, 2002, **36**, 527–538.

58 R. P. Schwarzenbach, P. M. Gschwend and D. M. Imboden, *Environmental Organic Chemistry*, John Wiley & Sons, Inc., 3rd Ed., 2016.

59 C. Ort, A. L. N. van Nuijs, J. D. Berset, L. Bijlsma, S. Castiglioni, A. Covaci, P. de Voogt, E. Emke, D. Fatta-Kassinos, P. Griffiths, F. Hernández, I. González-Mariño, R. Grabic, B. Kasprzyk-Hordern, N. Mastroianni, A. Meierjohann, T. Nefau, M. Östman, Y. Pico, I. Racamonde, M. Reid, J. Slobodnik, S. Terzic, N. Thomaidis and K. V. Thomas, Spatial differences and temporal changes in illicit drug use in Europe quantified by wastewater analysis, *Addiction*, 2014, **109**, 1338–1352.

60 A. K. McCall, R. Palmitessa, F. Blumensaat, E. Morgenroth and C. Ort, Modeling in-sewer transformations at catchment scale – implications on drug consumption estimates in wastewater-based epidemiology, *Water Res.*, 2017, **122**, 655–668.

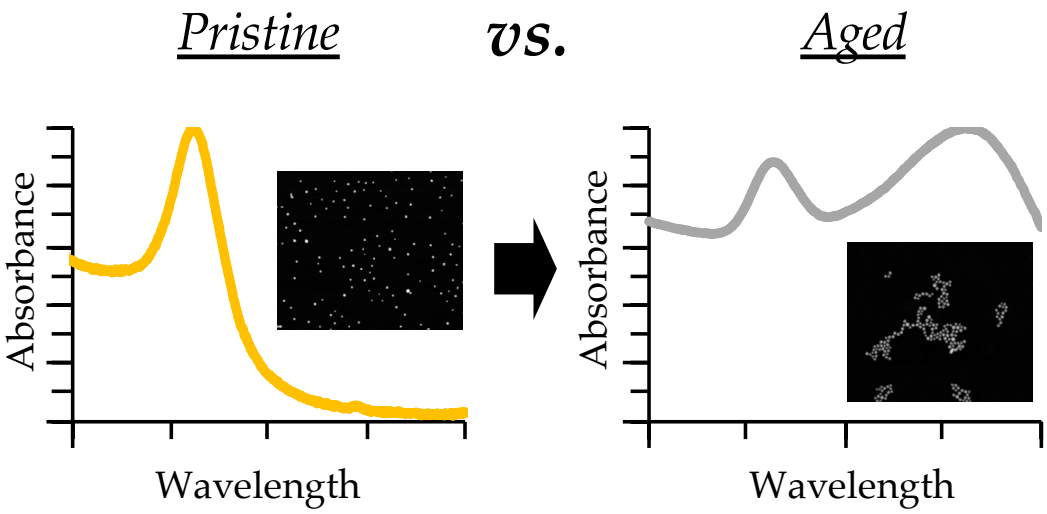

Engineered surface coatings alter ENM transformations (aggregation and corona formation) during conventional wastewater treatment processes.